Capacitively coupled double quantum dot system in the Kondo regime

Irisnei L. Ferreira, P. A. Orellana, G. B. Martins, F. M. Souza, and E. Vernek

Phys. Rev. B **84**, 205320 — Published 17 November 2011

DOI: 10.1103/PhysRevB.84.205320

Capacitively coupled double quantum dot system in the Kondo regime

Irisnei L. Ferreira,[1] P. A. Orellana,[2] G. B. Martins,[3,*] F. M. Souza,[1] and E. Vernek[1]

[1] *Instituto de Física - Universidade Federal de Uberlândia - Uberlândia, MG 38400-902 - Brazil*
[2] *Departamento de Física, Universidad Católica del Norte, Casilla 1280, Antofagasta, Chile*
[3] *Department of Physics, Oakland University, Rochester, MI 48309, USA*

A detailed study of the low-temperature physics of an interacting double quantum dot system in a T-shape configuration is presented. Each quantum dot is modeled by a single Anderson impurity and we include an inter-dot electron-electron interaction to account for capacitive coupling that may arise due to the proximity of the quantum dots. By employing a numerical renormalization group approach to a multi-impurity Anderson model, we study the thermodynamical and transport properties of the system in and out of the Kondo regime. We find that the two-stage-Kondo effect reported in previous works is drastically affected by the inter-dot Coulomb repulsion. In particular, we find that the Kondo temperature for the second stage of the two-stage-Kondo effect increases exponentially with the inter-dot Coulomb repulsion, providing a possible path for its experimental observation.

PACS numbers: 73.63.Kv, 72.10.Fk, 72.15.Qm, 73.23.Hk
Keywords: Double quantum dots, Kondo effect, Mixed valence regime, Coulomb blockade, Two-stage Kondo, Thermodynamics, Conductance, Capacitive coupling

I. INTRODUCTION

Many-body electron-electron interaction is one of the most striking phenomena in low dimension condensed matter systems. In this context, quantum dots[1] (QDs) have played a prominent role in the recent progress of theoretical studies,[2,3] as well as in experimental realizations,[4–8] as they offer a unique opportunity for successful measurement of many-body-related physical phenomena arising at low temperature regimes. The relevance of electron-electron interactions in QD systems results from the strong confinement of the electrons due to the reduced sizes of typical structures.[9–11] This interaction is responsible for several fascinating phenomena, e.g., Coulomb blockade,[11,12] and Kondo effect,[7,13,14] leading to characteristic behavior of the thermodynamical and transport properties, which depend drastically on the number of QDs, as well as on their topological configuration in the structure. In recent years, strong on-site interaction in double[13,15–24] and triple[25–32] QD (DQD and TQD) structures have received a great deal of attention when in the Kondo regime. However, *on-site* electron-electron interaction does not exhaust all the possibilities in multiple QD structures, as electrons can, due to their proximity, interact with each other, even when located in different QDs. It is important to note that recent advances in the lithography of lateral semiconductor QDs have allowed greater control over capacitively coupled DQD systems in parallel or in series.[33–37] This makes it even more relevant to better theoretically understand the effects of capacitive coupling over systems like the one studied in this paper. Only recently has this long-range interaction attracted more widespread attention of experimental and theory groups alike.[38–43]

The T-shape configuration, where two QDs are mutually coupled via a tunneling matrix element, while only one of them is coupled to metallic contacts, has attracted considerable interest as it allows the study of the two stage Kondo (TSK) effect, and interference phenomena as the Fano effect[23,44–47] by fine control of the inter-dot tunnel coupling. This effect results from the progressive screening of the localized spin of the electron in each QD as the system is cooled down to very low temperatures. Due to different effective couplings of the electron residing in each QD to the conduction band, these magnetic moments are screened at different temperature scales, which allows for the definition of two distinct Kondo temperatures. While the on-site Coulomb repulsion has received a great deal of attention, to the best of our knowledge the inter-dot Coulomb interaction in this particular system has not been considered yet. In this paper, we will explore how the TSK effect changes when a capacitive coupling is included between the dots. We will use the Numerical Renormalization Group (NRG) method[48–50] to calculate the transport and thermodynamical properties of the DQD system. We will show that this new ingredient is responsible for dramatic changes in the low-temperature physics of the system. In particular, as shown in Fig. 8, the Kondo temperature for the second stage of the TSK effect increases exponentially with the inter-dot Coulomb repulsion. This may have important consequences to the experimental observability of this effect.

The paper is divided as follows: In section II, we present the model and a brief description of the NRG method. In section III.A, we present numerical results for thermodynamical quantities (entropy and magnetic moment), for $U' = 0$. Results for finite U' are presented in section III.B, which is further subdivided in three subsections: subsection 1 contains thermodynamical results (entropy and magnetic moment), 2 contains results for QD occupancies and conductance at zero temperature, and subsection 3 contains results for the conductance dependence on temperature. Finally, in section IV, we

present our conclusions.

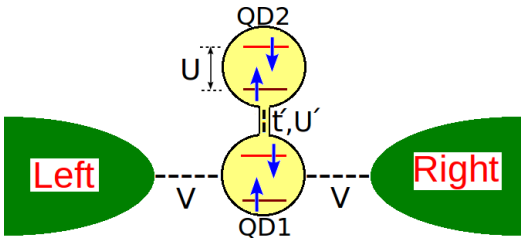

FIG. 1: (color online) Schematic representation of the DQD system being analyzed in this work. Note the capacitive interaction, U', between the dots.

II. THEORETICAL MODEL AND NUMERICAL METHOD

We study a system composed by two QDs (from now on referred to as QD1 and QD2) coupled by a tunneling matrix element as well as by capacitive inter-dot Coulomb repulsion. This system is described by the generalized Anderson Hamiltonian, which can be written as

$$H = H_{imp} + H_{cb} + H_{hyb}, \tag{1}$$

where H_{imp} is the Hamiltonian describing the QDs [which we define as "impurity region"], H_{cb} describes the conduction bands, and H_{hyb} describes the coupling of QD1 and the conduction bands (see Fig. 1). More explicitly,

$$\begin{aligned} H_{imp} &= \sum_{\substack{i=1,2\\ \sigma}} \varepsilon_i c^\dagger_{i\sigma} c_{i\sigma} + \sum_{i=1,2} U_i n_{i\uparrow} n_{i\downarrow} + U' n_1 n_2 \\ &\quad + t' \sum_\sigma \left[c^\dagger_{1\sigma} c_{2\sigma} + c^\dagger_{2\sigma} c_{1\sigma} \right], \end{aligned} \tag{2}$$

where the operator $c^\dagger_{i\sigma}$ ($c_{i\sigma}$) creates (annihilates) an electron in the i-th ($i = 1, 2$) QD, with energy ε_i, spin σ, $n_{i\sigma} = c^\dagger_{i\sigma} c_{i\sigma}$ is the number operator, and $n_i = \sum_\sigma n_{i\sigma}$. The second term in H_{imp} corresponds to the on-site Coulomb repulsion, where, for simplicity, we will take the intra-dot interactions $U_1 = U_2 = U$ throughout this paper. The third term describes the inter-dot Coulomb repulsion U' due to the proximity of the dots, and the last term describes the coupling between the two dots, with tunneling matrix element t'.

$$H_{cb} = \sum_{\ell k\sigma} \varepsilon_{\ell k} c^\dagger_{\ell k\sigma} c_{\ell k\sigma}, \tag{3}$$

where the operator $c^\dagger_{\ell k\sigma}$ ($c_{\ell k\sigma}$) creates (annihilates) an electron with momentum k, energy $\varepsilon_{\ell k}$, and spin σ in the ℓth lead ($\ell = L, R$). Finally,

$$H_{hyb} = \sum_{k\sigma} \left[V_{\ell k} c^\dagger_{1\sigma} c_{\ell k\sigma} + V^*_{\ell k} c^\dagger_{\ell k\sigma} c_{1\sigma} \right]. \tag{4}$$

While QD1 couples directly to the band, notice that QD2 couples to the band *indirectly* through QD1.

For simplicity, we assume the hybridization coupling $V_{\ell k} = V$ to be real, independent of k, and the same for both leads. The conduction band is characterized by a constant density of states given by $\rho_c(\omega) = \Theta(D - |\omega|)/2D$, where D is the half-bandwidth and $\Theta(x)$ is the standard Heaviside step function. To properly study the low-temperature physics of this setup we employ Wilson's NRG[48–50] approach, which allows for a systematic assessment of the Kondo effect in impurity systems. Within the NRG, we logarithmically discretize the conduction band and map it into a tridiagonal form, which corresponds to a semi-infinite chain where the coupling between the sites has the form

$$t_N = \frac{(1+\Lambda^{-1})(1-\Lambda^{-N-1})}{2\sqrt{1-\Lambda^{-2N-1}}\sqrt{1-\Lambda^{-2N-3}}}\,\Lambda^{-N/2}, \tag{5}$$

where Λ is the discretization parameter (all results shown here are for $\Lambda = 2.5$). The "impurity" site ($N = -1$) possesses sixteen degrees of freedom, corresponding to all the base-states necessary to fully describe the quantum state of the two QDs, while the other $N \geq 0$ sites correspond to single orbital non-interacting sites of Wilson's chain. Denoting the base-states of $H_{-1} = H_{imp}$ for the QDs as

$$|\,\phi_i\rangle_{-1} \equiv |\,m_1, m_2\rangle_{-1} \tag{6}$$

where $m_k = 1, 2, 3, 4$ corresponds, respectively, to $0, \uparrow, \downarrow$ or $\uparrow\downarrow$. In this basis the Hamiltonian H_{-1} has matrix elements

$$[H_{-1}]_{ij} = {}_{-1}\langle \phi_i \mid H_{-1} \mid \phi_j \rangle_{-1}. \tag{7}$$

By diagonalizing the matrix defined in Eq. 7 we obtain a set of sixteen eigenstates $\Psi_i\rangle_{-1}$ with corresponding eigenenergies $E_i^{(-1)}$. In terms of these base-states the eigenstates can be written as

$$|\,\Psi_i\rangle_{-1} = \sum_j A_{ij} \mid \phi_j\rangle_{-1}, \tag{8}$$

where A_{ij} is the projection of the ith eigenvector onto the j-th base-state. Once we obtain the eigenstates, we calculate all the necessary matrix elements for the next iteration, after which we add a new site $N = 0$. To describe the resulting system we enlarge the Hilbert space such that the new basis is constructed performing all 64 possible combinations

$$|\,\phi_i\rangle_0 := |\,m\rangle \otimes |\,\Psi_j\rangle_{-1}, \tag{9}$$

where $m = 1, \cdots, 4$ and $j = 1, \cdots, 16$. This procedure is repeated until the system has reached its strong-coupling fix point. When the dimension of the Hilbert space becomes larger than N_s, where typically $N_s = 2500$, it is truncated by discarding the eigenstates corresponding to the largest eigenenergies. At each iteration N we keep

the energy spectrum $E_i^{(N)}$, together with the matrix elements necessary to calculate the relevant physical quantities. This procedure allows us to calculate thermodynamical properties, such as entropy S_{imp}, magnetic moment $\mu_{imp}^2 = k_B T \chi_{imp}$, spin-spin correlation $\langle \mathbf{S}_1 \cdot \mathbf{S}_2 \rangle$, occupation numbers $n_{i\sigma} \equiv \langle n_{i\sigma} \rangle$, as well as dynamical quantities, like density of states (DOS) and conductance. For the entropy and magnetic moment it is usual to define the contribution from the impurity as S_{imp} and μ_{imp}^2. These quantities are generically written as $X_{imp} = X - X_0$, where X_0 is calculated in the absence of the impurity. Within the canonical ensemble, as a function of temperature T_N, we can write,

$$X(T_N) = \frac{1}{Z_N(T_N)} \sum_i {}_N\langle \Psi_i \mid \hat{X} \mid \Psi_i \rangle_N e^{-\beta_N E_i^{(N)}}, \quad (10)$$

where $\beta_N = (T_N)^{-1}$, and

$$T_N = \frac{1}{2 k_B \bar{\beta}} D (1 + \Lambda^{-1}) \Lambda^{-(N-1)/2} \quad (11)$$

is a characteristic temperature associated to the N-th iteration, $\bar{\beta}$ is a real number of order 1, $\hat{X}$ is the operator associated to the quantity X and

$$Z_N(T_N) = \sum_i e^{-\beta_N E_i^{(N)}} \quad (12)$$

is the canonical partition function.

The conductance is calculated by the generalized Landauer formula

$$G/G_0 = -\sum_\sigma \int_{-\infty}^{\infty} \mathtt{Im}[\mathcal{T}_\sigma(\omega)] \, [\partial f(\omega)/\partial \omega] \, d\omega, \quad (13)$$

where $\mathcal{T}_\sigma(\omega) = 2\pi V^2 \rho_c(\omega) G_{11}^\sigma(\omega)$, $G_0 = (2e^2/h)$ and $G_{11}^\sigma(\omega)$ is the Fourier transform of the full interacting double-time Green's function

$$G_{ii}^\sigma(t,t') = -i\Theta(t-t') \Big\langle \left[c_{i\sigma}(t), c_{i\sigma}^\dagger(t') \right] \Big\rangle, \quad (14)$$

which in the present case results to be (in the absence of magnetic field) spin independent. The Green's function is calculated at frequency $\omega_N = D(1+\Lambda^{-1})\Lambda^{-(N-1)/2}$ within NRG in a standard manner via Lehmann representation,

$$G_{ii}^\sigma(\omega_N) = \sum_{nn'} \frac{| \, {}_N\langle \Psi_n \mid c_{i\sigma} \mid \Psi_{n'} \rangle_N \, |^2}{\omega_N - \left(E_n^{(N)} - E_{n'}^{(N)} \right)} \times \left(e^{-\beta E_n^{(N)}} + e^{-\beta E_{n'}^{(N)}} \right). \quad (15)$$

We also employ a logarithmic Gaussian broadening[51] of the discrete NRG spectrum in order to obtain a smooth curve for the QDs DOS at arbitrary frequency ω

$$\rho_i^\sigma(\omega) = -\frac{1}{\pi} \mathtt{Im} G_{ii}^\sigma(\omega), \quad (16)$$

necessary to calculate the conductance at finite temperature.

III. NUMERICAL RESULTS

In order to proceed with our numerical analysis, let us set D, typically the largest energy scale of the problem, as our energy unit ($D = 1$). We then choose for all calculations $U_1 = U_2 = U = 5 \times 10^{-4}$ and $V = 3.2 \times 10^{-3}$, so that $U/\pi\Gamma_1 \approx 5$, where $\Gamma_1 = 2\pi V^2 \rho_0$, and $\rho_0 = 1/(2D)$. We will study in detail the two cases where $U' = 0$ and $U' = U$, and also the range $0 < U/U' < 1$. The bare levels ε_1 and ε_2 will be controlled by the same gate voltage (V_g), such that $\varepsilon_1 = \varepsilon_2 = V_g$. With the parameters set above, and $V_g = -(U/2 + U')$ (i.e., with the system at the particle-hole (p-h) symmetric point), we can estimate the Kondo temperature for the single QD as[49] $T_K = \sqrt{\Gamma_1 U} \exp(-\pi U/8\Gamma_1) \approx 2.89 \times 10^{-7}$ for QD1, when QD2 is completely disconnected ($t' = 0$ and $U' = 0$).

A. $U' = 0$ case

Although this case has been studied in great detail in Ref. 23, we will present below some results that will help us understand the more complicated situation at finite U'. In Figs. 2 and 3, we show results for the temperature dependence of the entropy (Fig. 2) and the square of the total magnetic moment (Fig. 3) of the DQD system, $S_{imp}/k_B \ln(2)$ and $\mu_{imp}^2/(g\mu_B)^2$, for $U' = 0$, $\varepsilon_1 = \varepsilon_2 = -U/2$, and various values of t', where k_B is Boltzmann's constant and μ_B is the Bohr magneton. For the special case where $t' = 0$ [(black) $\circ$ curve], the DQD corresponds to the case where just QD1 is coupled to the conduction band and QD2 is completely decoupled from the rest of the system.[52] In this situation, as the temperature decreases, we find the following regimes: *(i)* for $k_B T \gg U$ the DQD is in its free orbital (FO) regime; in this regime, the temperature is high enough to allow for all the sixteen DQD states to be populated. This results in an entropy $S_{imp} = k_B \ln(16)$ (see Fig. 2) and a total square magnetic moment $\mu_{imp}^2 = 2 \times (g\mu_B)^2/8$ (Fig. 3), *(ii)* for $k_B T_K < k_B T < \varepsilon_1, \varepsilon_2$, thermally excited charge fluctuations are suppressed, and therefore the entropy decreases to $S_{imp} = k_B \ln(4)$, as only states with one electron in each QD are favored (providing four states; the two states with both electrons in the same QD, either QD1 or QD2, have higher energy). This implies that μ_{imp}^2 increases, as double and unoccupied states in each QD are suppressed, and the DQD is in the so-called local moment (LM) regime. As the temperature further decreases, and becomes lower than T_K, QD2 remains in its LM regime (and, for $V_g = -U/2$, is singly occupied), while the other spin (in QD1) is progressively screened by the conduction electrons due to the formation of the Kondo state. This regime is characterized by the plateaus $S_{imp} = k_B \ln(2)$ and $\mu_{imp}^2 = (g\mu_B)^2/4$. These contributions arise just from the spin in QD2, as it is never Kondo screened when $t' = 0$.

For finite t', however, the behavior of the DQD for

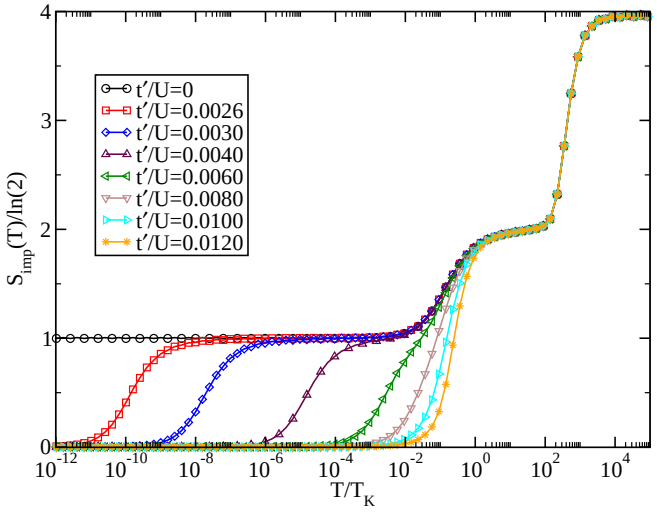

FIG. 2: (color online) Temperature variation of the entropy for various values of t' (see legend). The other parameters are $U_1 = U_2 = 5 \times 10^{-4}$, $U' = 0$, $\varepsilon_1 = \varepsilon_2 = -2.5 \times 10^{-4}$, and $V = 3.2 \times 10^{-3}$. Note that the temperature in the horizontal axis is scaled by the Kondo temperature of QD1 (see text), which, for the parameters chosen, is $T_K = 2.89 \times 10^{-7}$. Details for the different regimes are provided in the text.

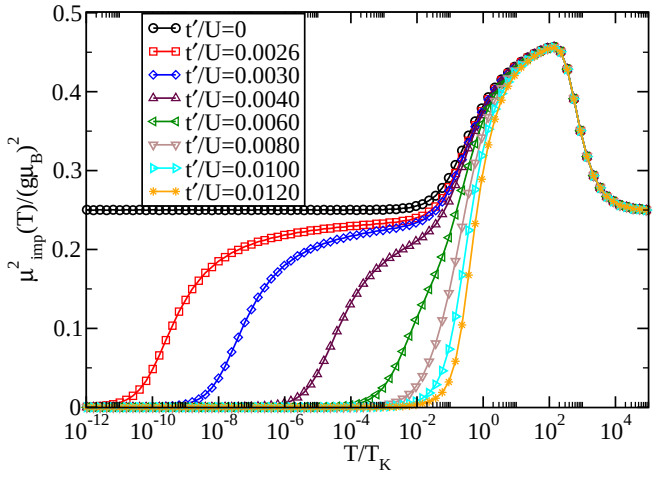

FIG. 3: (color online) Magnetic moment $k_B T\chi$ as function of temperature for various values of t'. All parameters are the same as in Fig. 2.

temperatures below T_K is quite different from the one just described above for $t' = 0$. For very small values of t', as shown in Ref. 23, the DQD system presents a TSK effect, where *both* QD1 and QD2 spins are screened by the conduction band, but the screening of the spin in QD2 occurs at a much lower temperature than that at which the spin in QD1 is screened. The second screening stage emerges at a characteristic temperature T'_K which depends mainly upon t' and T_K (the Kondo temperature for QD1) as

$$T'_K = a T_K \exp\left(-b T_K / J'\right), \tag{17}$$

where a and b are real positive numbers, with values of $\mathcal{O}(1)$,[23] and $J' = 4t'^2/U$ is an effective antiferromagnetic coupling (between electrons in QD1 and QD2) favoring a local singlet state that competes with the regular Kondo energy scale T_K. As a result, a TSK effect is expected for $J' < T_K$. We can clearly see this behavior, for example, when $t'/U = 0.0026$ [(red) □ curve] in Figs. 2 and 3. Note that for this value of t'/U the second drop in the entropy (signaling the screening of the electron in QD2) happens at $T'_K \approx 10^{-17}$, with $J' \approx 1.35 \times 10^{-8}$ (for this value of t') being much larger than T'_K, but smaller than T_K (remember that $T_K \sim 2.89\ 10^{-7}$). As t' increases, and eventually J' becomes larger than T_K, a strong singlet is formed locally, destroying the TSK picture. A detailed discussion of this crossover can be found in Ref. 23; here, instead, we focus on the effect of the inter-dot Coulomb repulsion, as discussed in the next section.

B. Finite U'

1. *Entropy and magnetic moment*

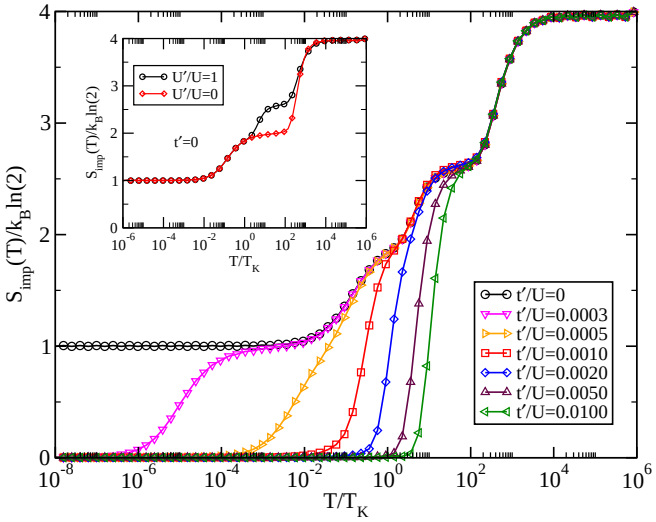

FIG. 4: (color online) Same as in Fig. 2, but now for $U' = U$ and different values of t' (see legend). The Kondo temperature used to scale the horizontal axis is that obtained for $U' = U$ and $t' = 0$. The inset contains a comparison of $t' = 0$ results between $U' = 0$ [(black) ○ curve] and $U' = U$ [(red) ◇ curve], showing that the Kondo temperature of the first stage (for $t' = 0$) does not depend on U'.

Now, we turn on U' and for simplicity we choose $U' = U$ (later on, we will analyze results for $0 < U' < U$). The new features to note in the entropy, Fig. 4, in relation to the results in Fig. 2, for $U' = 0$, are *(i)* the very clear plateau (in Fig. 2) at $S_{imp}/k_B \ln(2) = 2$ splits into

two narrower plateaus in Fig. 4: one at $S_{imp}/k_B \ln(2) \approx 2.66$, and the one at $S_{imp}/k_B \ln(2) = 2$ becomes less well defined, more like a shoulder. The plateau at $\approx \ln(6)/\ln(2) = 2.58$ (starting at $T \approx 10^2\ T_K$) comes from the fact that now, as $U' = U$, all 6 states with 2 electrons have very similar energies. As the temperature goes further down, the 4 states that can participate in a Kondo state in QD1 (one electron in each QD) will have lower energy and the shoulder around $S_{imp}/k_B \ln(2) = 2$ will form (at $T \approx T_K$), *(ii)* to obtain the second stage of the TSK (signaled by the suppression of the plateau at $S_{imp}/k_B \ln(2) = 1$, for finite t') one needs to go to one order of magnitude smaller values of t', when compared to the results for $U' = 0$ (compare the (purple) $\triangle$ curve in Fig. 2, for $t' = 0.004$, with the (purple) $\triangle$ curve in Fig. 4, for $t' = 0.005$, where all traces of the second stage in the TSK effect have vanished), *(iii)* it is also apparent that, contrary to the $U' = 0$ case, T'_K depends much more strongly on t'. Indeed, it is clear that the temperature at which the entropy starts to decrease to zero becomes considerably higher as t' increases, in contrast to what can be seen in Fig. 2. It is important to note that the horizontal axis in Fig. 4 is scaled by the Kondo temperature (for QD1) for $t' = 0$, estimated with the expression in the text above (at the beginning of section III). In the inset to Fig. 4 we show that T_K for $U' = 0$ and for $U' = U$ are equal: Indeed, this is illustrated in the inset by the agreement between the entropy curves (for $T < T_K$) calculated for $t' = 0$ [(black) $\bigcirc$ curve for $U' = U$, and (red) $\diamond$ curve for $U' = 0$].

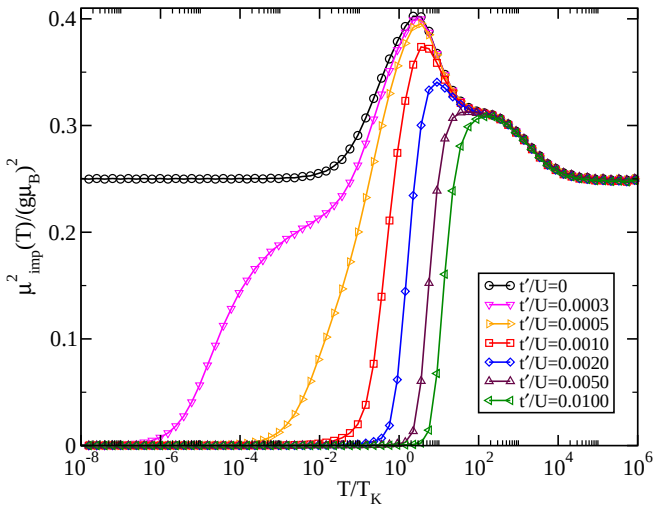

FIG. 5: (color online) Magnetic moment $k_B T\chi$ as function of temperature for various values of t'. All parameters are the same as in Fig. 4.

In relation to the magnetic moment (Fig. 5), a few differences are quite apparent when U' is turned on: *(i)* as t' decreases, the peak in the susceptibility moves from $T/T_K \approx 10^2$ to $T/T_K \approx 1$. As seen in the entropy results, at $T/T_K \approx 10^2$ the 2 states with both electrons in the same QD have the same energy as the ones with one electron in each QD, and therefore the square of the magnetic moment is smaller. As the temperature decreases towards T_K, the DQD will start to form the Kondo state, lowering the energy of the states where QD1 is single occupied, thus increasing the square of the magnetic moment; *(ii)* as discussed in the case of $U' = 0$, for the 3 larger values of t', a strong local singlet is formed ($J' > T_K$) and both Kondo stages are suppressed, and the magnetic moment starts to decrease for $T > T_K$.

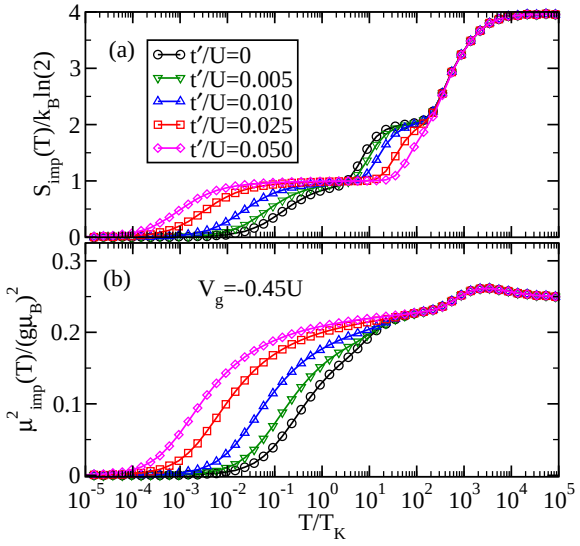

FIG. 6: (color online) (a): Entropy and (b): Magnetic moment, as a function of temperature for various values of t' (see legend). All parameters are the same as in Fig. 4, except that now the results are for a gate potential value ($V_g/U = -0.45$) away from the p-h symmetric point (i.e., $V_g/U = -3/2$).

For the sake of completeness, in Fig. 6, we show the entropy [panel (a)] and the magnetic moment [panel (b)] at $V_g/U = -0.45$, i.e, when the system is away from the p-h symmetric point. Figure 6(a) shows the entropy for $t' = 0$, 5×10^{-3}, 1×10^{-2}, 2.5×10^{-2}, and 5×10^{-2} [(black) $\bigcirc$, (green) $\triangledown$, (blue) $\triangle$, (red) $\square$, and (magenta) $\diamond$, respectively). For this relatively high value of gate potential, states with 2 and 3 electrons (with 6 and 4 states, respectively) have high energy and do not form a plateau below the 4 electron plateau (with 16 states). The plateau formed at $10^2 \times T_K$ corresponds to single occupancy of the DQD (with four possible states). Note that this plateau is only stable for the two lower values of t' (besides $t' = 0$). Let us analyze first the results for these lower values of t': As the temperature goes down, to around $10 \times T_K$, states where only QD1 is occupied become more favorable (as they will participate in the formation of the Kondo state). This gives origin to the plateau at $ln(2)$, which will start to be suppressed once the Kondo singlet is formed (at $T \approx T_K$, for $t' = 0$). Note that as t' becomes finite and increases, the Kondo screening will occur at a lower T_K, and therefore the plateau at $ln(2)$ will become broader. The decrease in T_K occurs because now the magnetic moment becomes

more delocalized and the screening by the Fermi sea is less efficient. Finally, as t' further increases, the plateau at $ln(4)$ is suppressed and the system goes straight to the plateau with two states $[ln(2)]$. This is a manifestation of the formation of molecular orbitals.[53] The value of T_K obtained for the higher values of t' decreases even further: for example, for $t' = 5 \times 10^{-2}$, T_K decreases by $\approx 10^{-3}$ of the T_K value obtained for $t' = 0$. This decrease occurs because the effective Γ connecting the molecular orbital to the band is smaller than Γ_1 (coupling of ε_1 to the band for $t' = 0$). A similar analysis can be done of the magnetic moment results in Fig. 6(b).

However, the most important differences coming from adding U' are related to the behavior of T_K and T'_K. First, the value of T_K being used for the scaling of the horizontal axis (in Figs. 2 to 5) is that obtained when $t' = 0$. Note from Figs. 2 and 3, that T_K is very weakly dependent on t' when $U' = 0$. That is clearly not the case for $U' = U$, where it can be seen a strong variation of T_K and T'_K with t'. In addition, more interestingly from an experimental point of view, it is clear that the ratio T'_K/T_K increases by a few orders of magnitude for $U' = U$.

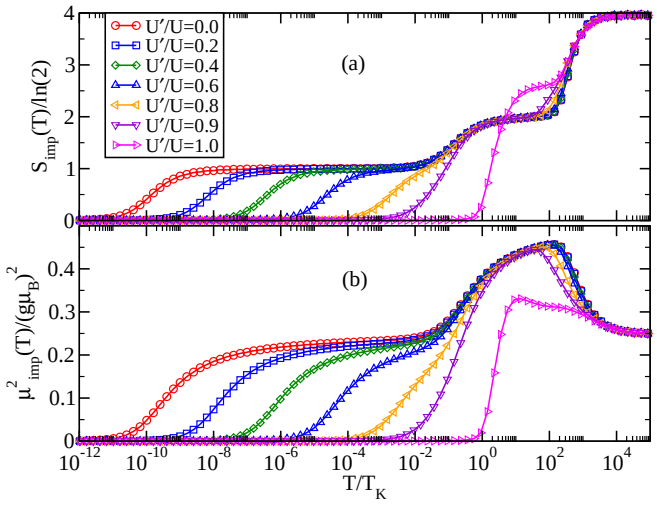

FIG. 7: (color online) (a) Entropy S_{imp} and (b) Magnetic moment $k_B T\chi$ as function of temperature for various ratios of U'/U (between 0 and 1, see legend) for $t'/U = 0.0026$. To preserve the p-h symmetry for each curve we set $V_g = -U/2 + U'$. All the other parameters are the same as in Figs. 4 and 5. It is clear from the results that the Kondo temperature for the second stage of the TSK effect is greatly enhanced (by a few orders of magnitude) when U' increases.

To analyze in more detail the increase of T'_K with U' we show, in Fig. 7, results for entropy [panel (a)] and magnetic moment [panel (b)] which clearly indicate the strong increase in T'_K (by a few orders of magnitude) when the ratio U'/U varies from 0 to 1 for a fixed value of $t'/U = 0.0026$. This increase in T'_K can be understood by estimating the Kondo temperature T'_K for the second stage of the TSK, by using eq. 17 to estimate T'_K, and

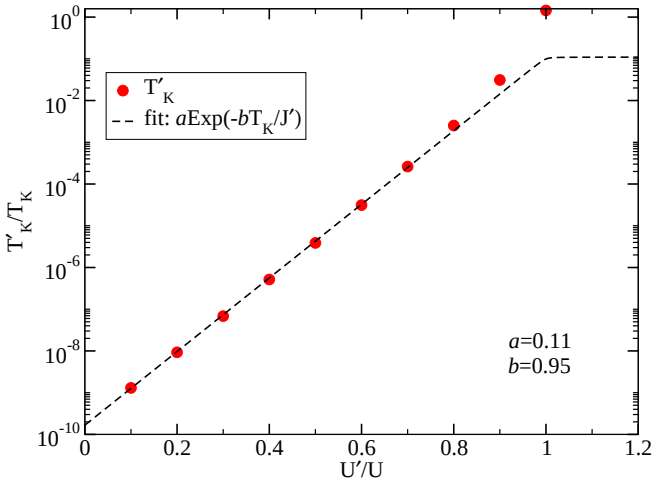

FIG. 8: (color online) Fitting (dashed line) of the T'_K values [red dots] extracted from Fig. 7, obtained by using eqs. 17 and 18. The values obtained (from the fitting) for the two free parameters a and b are indicated in the figure.

explicitly calculating J' for finite U':

$$J' = -\frac{U - U' - \sqrt{(U-U')^2 + 16t'^2}}{2}, \qquad (18)$$

indicating that, at least for small values of U'/U [where $J' \sim 4t'^2/(U-U')$], there should be an exponential increase of T'_K with U'/U. This expectation is supported by the NRG results shown in Fig. 7. One can go one step further by substituting eq. 18 into eq. 17, and use the equation thus obtained to fit the values of T'_K that can be extracted from Fig. 7. This fitting is shown in Fig. 8. Note that the only free parameters are 'a' and 'b' (values indicated in the figure). It can be clearly seen that the fitting, at least up to $U'/U \sim 0.7$, is very good (note that the vertical axis is in a logarithmic scale). Indeed, this is one of the principal results of this paper. Given the recent advances in the use of floating interdot capacitors (see Ref. 33), values of U'/U for double dot systems have been steadily increasing, and may, in light of our results, offer the hope of observing the so far experimentally inaccessible energy scale T'_K.

2. *Zero-temperature case: QD occupation and conductance*

We first study how the occupation of the dots, $\langle n_i \rangle \equiv \sum_\sigma \langle n_{i\sigma} \rangle$, is modified due to inter-dot Coulomb repulsion. In Fig. 9, we show $\langle n_2 \rangle$ (top) and $\langle n_1 \rangle$ (bottom) as function of V_g for various values of t'. For $t' = 0$ [(black) ○ curve], at $V_g \approx 0$ one can observe a smooth increase of $\langle n_1 \rangle$, while $\langle n_2 \rangle$ remains zero all the way down to $V_g/U \approx -0.5$, where $\langle n_2 \rangle$ jumps to 1 and $\langle n_1 \rangle$ abruptly decreases. The value of V_g for which the first discontinuity of $\langle n_2 \rangle$ occurs (expected to be at $V_g \approx 0$, when $U' = 0$) depends on the additional capacitive energy necessary to put electrons in different

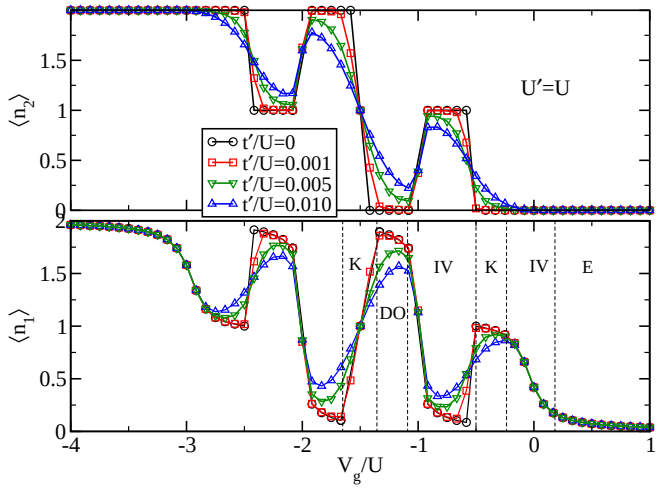

FIG. 9: (color online) Total occupation $\langle n_2\rangle$ (top) and $\langle n_1\rangle$ (bottom) as function of gate voltage (V_g) for $t'/U = 0$ (○), $t'/U = 1.0\times10^{-3}$ (□), $t'/U = 5\times10^{-3}$ (◇) and $t'/U = 1.0\times10^{-2}$ (△). Other parameters are $t'/U = 5\times10^{-4}$, $V = 3.2\times10^{-3}$, and $U = U'$. The regions delimited by the vertical lines in the bottom panel refer to QD1 states, namely, empty (E), intermediate valence (IV), Kondo (K) and doubly occupied (DO) intermediate valence.

dots, due to the inter-dot Coulomb repulsion U'. Note that all the charge occupancy and conductance curves, as a function of V_g (in Figs. 9, 10, 11, and 13), for $V_g/U < -(U/2+U')/U = -3/2$ were obtained by p-h symmetry from those calculated for $V_g/U > -3/2$.

As discussed by three of the current authors in a previous work,[54] this gate-voltage-dependent charge oscillation can be understood as a competition between the Kondo and Intermediate Valence (IV) regimes:[55] level ε_2, when $t' = 0$, acts as a dark state, whose charge occupation, which can only be an integer, adds a step function of height U' to the gate potential V_g in QD1 (depending on $\langle n_2\rangle$ being 0 or 1). The value of V_g for which the transition of $\langle n_2\rangle$ between 0 and 1 (and vice versa) occurs depends on Γ_1 and reflects which many-body regime, Kondo or IV, better optimizes the energy of QD1. The dark state ε_2 acts like a switch between the two regimes and may have applications in quantum computation.[54,56] For example, when the first discontinuity occurs, for $V_g/U \approx -0.5$, QD1 is in a Kondo state, however, a further decrease of V_g makes it *energetically* more favorable for QD1 to be in an IV state, which can be accomplished by charging QD2 (by exactly one electron), this, due to the capacitive coupling, increases the effective gate potential of QD1, discharging it, and bringing it back to the IV regime.[57] As V_g/U further decreases below -0.5, QD1 starts to transition from an IV to a Kondo state; when $V_g/U \approx -1$, again the IV state for QD1 is more favorable; this regime can now be achieved by completely avoiding the Kondo regime through the discontinuous charging of QD1 by one extra electron. Total charge is kept constant by discharging QD2 completely ($\langle n_2\rangle = 0$). Finally, further decrease of V_g, bringing it close to the p-h symmetric point [$V_g = -(U/2+U') = -3U/2$], increases the charge in QD1 to almost 2 electrons; at this point, the Kondo state in QD1 is more favorable, and a new discharging and charging occurs of QD1 and QD2, respectively, after which, each QD hosts one electron. These gate-voltage-dependent occupancy oscillations are clearly observed for all curves in Fig. 9, with the difference that, for finite t', there are no discontinuities. we rather notice that the jumps are smoothened out as t' increases. This continuous charging of QD2 now results from the broadening Γ_2 of the local bare (and also the many-body) level at QD2. For the non-interacting case it is easily shown that $\Gamma_2 \propto t'^2\Gamma_1$. It is important to note the differences and similarities between this model and the one studied in Ref. 54: in the latter, one has a two channel system, where the dark state, for small values of t_-, acquires a finite broadening and smoothens out the discontinuities seen in the $\langle n_1\rangle$ and $\langle n_2\rangle$ curves in Fig. 9. In the model being studied here, a similar process occurs: the dark state in QD2 acquires a broadening through its connection t' to the *single* conduction channel *through* QD1. Nonetheless, through a comparison of Fig. 9 in this work with Fig. 5 in Ref. 54 [panels (c) and (d)], one can see that qualitatively the results are very similar, indicating that the basic processes determining the gate voltage dependent occupancy oscillations are the same.

The strong gate-voltage-dependent variations in $\langle n_i\rangle$ ($i = 1,\ 2$) (*caused by the capacitive coupling*) are expected to have dramatic influence in the conductance of the system, specially in the Kondo regime (see Fig. 10). For $U' = 0$, and in the special case where $t' = 0$, QD1 will be in a Kondo state for all V_g values in the interval $[-U, 0]$. For finite U', however, the charging and discharging of the QDs moves QD1 from a Kondo to an IV regime, and vice versa (as described above). For $t' = 0$ (panel (a) in Fig. 10), when V_g becomes negative, we observe a narrow Kondo plateau of height G_0, and then the conductance drops suddenly to almost zero at $V_g/U \approx -0.5$, which is exactly the gate potential value where QD1 is discharged (see Fig. 9). This drop signals the transitioning of QD1 from the Kondo to the IV regime, as described above and in Ref. 54. The small peak (of height $\approx 0.3\ G_0$) observed at $V_g/U \approx -1$ corresponds to the discontinuous jump of the renormalized level $\tilde{\varepsilon}_1 \approx \varepsilon_1 + U'\langle n_2\rangle$, caused by the discontinuous change in $\langle n_2\rangle$ from 1 to 0, leading QD1 from a low occupancy ($\langle n_1\rangle \approx 0.0$) IV regime, to a high ($\langle n_1\rangle \approx 2.0$) IV regime, completely skipping the Kondo regime (with occupancy $\langle n_1\rangle \approx 1.0$).

When the system reaches the vicinity of its p-h symmetric point [$V_g = -(U/2+U') = -3U/2$], there are exactly two electrons in the QDs (one in each) and the Kondo effect is fully reestablished in QD1 (for $t' = 0$), thus the conductance reaches G_0. Due to p-h symmetry, the other half of the curve can be explained in a similar way. The curve in panel (a) of Fig. 10 should be compared to the right-side panel of Fig. 3(b) in Ref. 54.

For increasing t' (panels (b) to (d) in Fig. 10) there

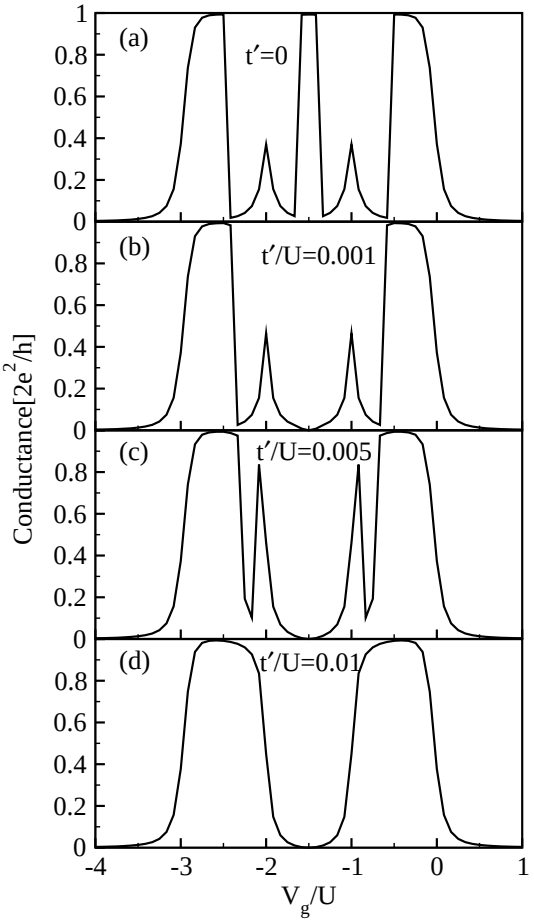

FIG. 10: Zero-temperature conductance as a function of V_g for the same parameters as in Fig. 9. The conductance discontinuities seen here are directly related to the occupancy discontinuities observed in Fig. 9. See text for a full description of the variation of the peak structures with increasing t': (a) $t'/U = 0$, (b) $t'/U = 10^{-3}$, (c) $t'/U = 5 \times 10^{-3}$, and (d) $t'/U = 10^{-2}$.

are mainly two differences in the charge and in the conductance: *i)* the abruptness of the charging/discharging and the discontinuities in the conductance are progressively smoothed out, and *ii)* the central peak in the conductance (around the *p-h* symmetric point) is fully suppressed. For example, for $t'/U = 1 \times 10^{-3}$, a rapid drop in the QD occupations is still clearly visible (as observed on the □ (red) curve in Fig. 9), resulting in a rapid variation in the conductance, which now moves down to a lower value of V_g when compared with the $t' = 0$ curve (see panel (b) in Fig. 10). Notice that the peak at $V_g \approx -U$ is enhanced, as t' increases, and the position of the peak moves up to higher gate potential values. For $t' = 1 \times 10^{-2}$ the discontinuity is fully suppressed and one obtain a typical Kondo plateau centered at $V_g = -U/2$. This starts to mark the transition to the molecular regime, which, as stated above, has a very broad crossover region between very small and very large values of t'.[53] The suppression of the conductance around the *p-h* symmetric point for small (but finite) t' results from destructive Fano-like interference due to the Kondo resonance in QD2. For large t', on the other hand, this suppression results from the formation of a local singlet due to an antiferromagnetic effective coupling ($J = 4t'^2/U$) between the two electrons in the QDs, competing with the Kondo singlet formed between the electron in QD1 and the conduction electrons. This is clearly associated to the TSK effect previously analyzed in this system.[23]

One should note that there is a striking difference in the effect of t' over the conductance for different regions of gate potential, and for different values of t'. For the smallest value studied ($t'/U = 1 \times 10^{-3}$), as mentioned above, the Kondo peak at half-filling is immediately suppressed and this can be associated to the TSK effect. On the other hand, the peak around $V_g = -U$ is barely affected for a small t'. Indeed, as the TSK effect depends on the energy scale J', one expects that it will be more effective at half-filling. Higher values of t' will then quickly modify the structures around $V_g = -U/2$ and $V_g = -U$: the peak at $V_g = -U$ is quickly enhanced, while the discontinuity located at $V_g \approx -U/2$ (for $t' = 0$) moves to lower gate potential values, extending the Kondo plateau, until the two structures merge and form a single Kondo peak centered at $V_g = -U/2$. This occurs because now level ε_2 acquires a finite width and therefore the discharging of QD1 (and simultaneous charging of QD2) is not abrupt anymore and the system smoothly proceeds from the IV regime (with $\langle n_1 \rangle < 1$), to the Kondo regime (with $\langle n_1 \rangle \approx 1$), and back to the IV regime (with $\langle n_1 \rangle < 1$ again). This can be clearly seen by observing the (blue) △ curve in Fig. 9 (lower panel) and the curve in Fig. 10(d). As mentioned above, this also marks the beginning of the crossover to the molecular regime.

3. Finite-temperature case

Now we turn our attention to the effect of temperature in the transport properties of the system described in Fig. 1. In Fig. 11, we show the conductance for $U' = U$, $t'/U = 1.0 \times 10^{-3}$, and various values of temperature. The curves in this figure should be compared to the corresponding zero temperature curves in Fig. 10 [panel (b)]. Starting with $T/T_K = 1.7 \times 10^{-3}$ [(black) △ curve] we notice a very similar shape when compared to the $T = 0$ results in Fig. 10 [panel (b)], except that the two symmetric Kondo plateaus and the IV peaks at $V_g/U \approx -1$ and $V_g/U \approx -2$ are slightly suppressed, which results from the small (but finite) temperature. Results for smaller temperatures (not shown) interpolate between $T = 0$ and $T/T_K = 1.7 \times 10^{-3}$. For $T/T_K = 1.66 \times 10^{-1}$ [(red)

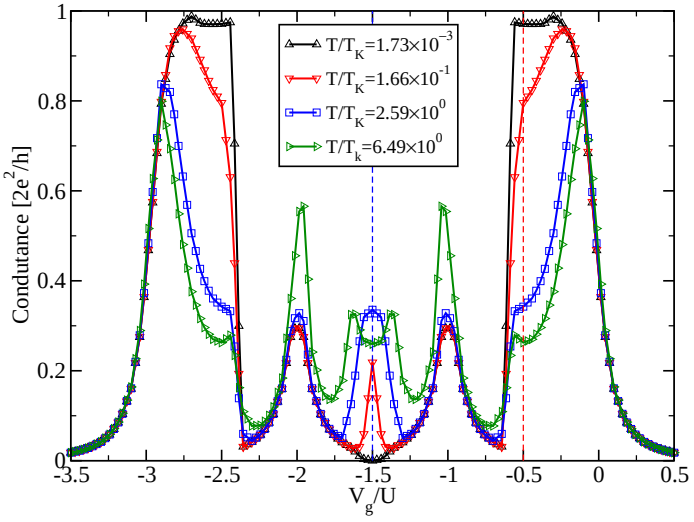

FIG. 11: (color online) Conductance as function of V_g for $U' = U$, $t'/U = 1.0 \times 10^{-3}$ and for different temperatures: $T/T_K = 1.73 \times 10^{-3}$ [(black) $\triangle$], $T/T_K = 1.66 \times 10^{-1}$ [(red) $\triangledown$], $T/T_K = 2.59$ [(blue) $\square$], $T/T_K = 6.49$ [(green) $\triangleright$].

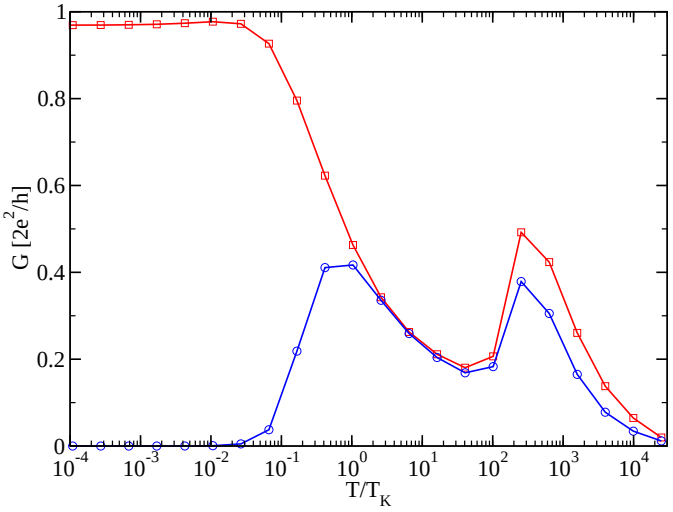

FIG. 12: (color online) Conductance as function of temperature for $t'/U = 1.0 \times 10^{-3}$ for $V_g/U = -1.5$ [(blue) $\bigcirc$] and $V_g = -0.5$ [(red) $\square$], along the (blue and red) dashed vertical lines shown in Fig. 11.

$\triangledown$ curve] we observe a clear suppression of the Kondo plateau, while the IV peaks do not differ much from those for lower temperatures. This is readily understood, as the characteristic energy of the Kondo state T_K is much smaller than the energy scale associated to the IV regime, of order Γ_1 (for details, see Fig. 8 in Ref. 54). On the other hand, it is interesting to notice the emergence of a sharp small peak at the p-h symmetric point for a higher temperature such as $T/T_K = 1.66 \times 10^{-1}$ [(red) $\triangledown$ curve]. This peak results from a revival of the Kondo peak observed for $t' = 0$ in the $T = 0$ case, see the corresponding curve in Fig. 10(a). This revival of the Kondo peak results from the suppression of the second stage Kondo effect (for $T > T'_K$), allowing the Kondo effect in QD1 to be seen through a zero bias anomaly in the conductance. On the other hand, for $T > T_K$, as in the (green) $\triangleright$ curve, we observe a suppression of the p-h symmetric Kondo peak, similar to a splitting.

In order to show this effect in more detail, in Fig. 12 we plot the temperature variation of the conductance for the same parameters as in Fig. 11, for two different values of V_g. For $V_g/U = -1.5$ [(blue) $\bigcirc$ curve], the conductance vanishes when $T \to 0$, increases for $10^{-2} \lesssim T/T_K \lesssim 10^0$, and is suppressed again for $T \gtrsim T_K$. Note that the initial enhancement of the conductance as the temperature increases results from the destruction of the Kondo resonance in the QD2, suppressing the destructive interference between the two paths. Conversely, as the temperature keeps increasing, and T exceeds T_K, the conductance is suppressed due to the destruction of the Kondo resonance in QD1. Finally, it will rise again and reach a maximum at approximately $T/T_K \sim 10^2 \approx \Gamma_1$ due to charge fluctuations in QD1. For $V_g/U = -0.5$ [(red) $\square$ curve], i.e., at the edge of the right plateau of Fig. 11], the conductance starts from $G_0 = 2e^2/h$ as $T \to 0$, and is suppressed for $10^{-2} \lesssim T/T_K \lesssim 10$ due to the destruction of the Kondo effect in QD1. This is the behavior of the regular Kondo effect in a single QD. It is interesting to point out that once the temperature is above T_K, the conductance at both V_g values behave alike.

In Fig. 13, similarly to Fig. 11, we show G *vs.* V_g, for different temperatures, but now for $t' = 1 \times 10^{-2}$, the largest t' value used in Fig. 10, for which the two QDs form so-called molecular orbitals.[53] These curves should be compared to the zero-temperature curve in Fig. 10(d). For the case of $T/T_K \sim 10^{-10}$ [(red) $\bigcirc$ curve], it has the same shape as the corresponding curve in Fig. 10(d). We notice, however, that by gradually increasing the temperature, both Kondo plateaus become valleys surrounded by two Coulomb blockade peaks, while the gap at the p-h symmetric point remains almost unchanged. This is consistent with what one would expect of the charge transport at high temperature for two molecular levels.

IV. CONCLUDING REMARKS

We have studied a strongly interacting double dot system arranged in a T-shape configuration, where the dots are coupled via a tunneling matrix element and also strong inter-dot Coulomb repulsion. We have presented a detailed study of the effect of the inter-dot Coulomb interaction on the Kondo physics of the system. Our numerical analysis reveals interesting crossovers between different mixed valence and Kondo regimes that produce dramatic changes in the conductance of the system. These crossovers can be tuned by varying the gate voltage of the QDs, and the charging/discharging processes produce anomalous peaks in the conductance across the system, allowing a clear identification of the

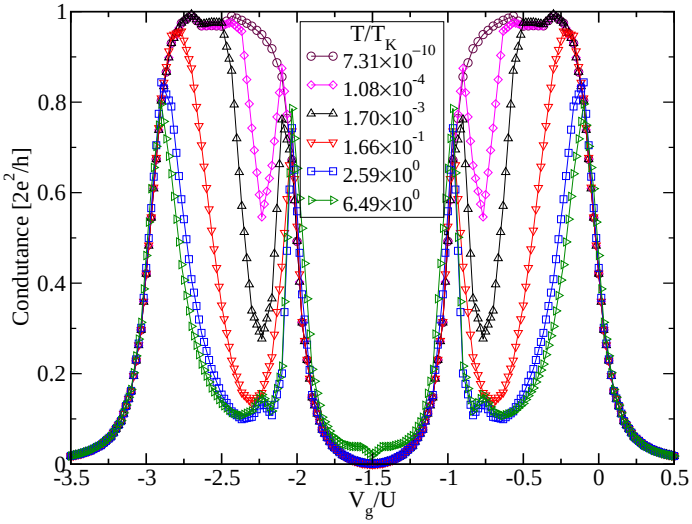

FIG. 13: (color online) Conductance as function of V_g and $t'/U = 0.01$ for various temperatures: $T/T_K = 7.31 \times 10^{-10}$ ($\bigcirc$), $T/T_K = 1.08 \times 10^{-4}$ ($\diamond$), $T/T_K = 1.70 \times 10^{-3}$ ($\triangle$), $T/T_K = 1.66 \times 10^{-1}$ ($\triangledown$), $T/T_K = 2.59 \times 10^{0}$ ($\square$), and $T/T_K = 6.49 \times 10^{0}$ ($\triangleright$).

various regimes. We show that the inter-dot Coulomb repulsion not only preserves the TSK regime, but it also dramatically increases the lowest energy scale of the TSK effect. Indeed, T'_K increases exponentially with the inter-dot Coulomb interaction, as shown in panels (a) and (b) of Fig. 7. We stress that this enhancement may allow the experimental observation of this so far elusive effect. In addition, by fixing the gate voltage at the p-h symmetric point and raising the temperature, the conductance shows clearly the crossover from TSK to Kondo and then to mixed valence regime (see Fig. 12, (blue) $\bigcirc$ curve). By contrast, away from the p-h symmetry only the regular Kondo regime is observed. For temperatures larger than T_K (and large enough values of the coupling t' between the QDs) the conductance of the system as a function of the gate voltage possesses a four-peak structure, showing clearly the Coulomb blockade regime of the molecular orbitals of the system. Finally, we believe that our results will motivate future experimental measurements in capacitively coupled T-shape QD geometries.

Acknowledgments

ILF, FMS, and EV acknowledge CNPq, CAPES, and FAPEMIG, the Brazilian agencies, for financial support. PO acknowledges FONDECYT under grant No. 1100560, and GBM acknowledges financial support by the National Science Foundation under Grant No. DMR-0710529. We also would like to thank G. A. Lara for valuable discussions.

* Corresponding author: martins@oakland.edu

[1] M. Reed, Scientific American **268**, 118 (1993).
[2] M. Kulkarni and R. M. Konik, Phys. Rev. B **83**, 245121 (2011).
[3] T. Kubo, Y. Tokura, and S. Tarucha, Phys. Rev. B **83**, 115310 (2011).
[4] S. M. Cronenwett, T. H. Oosterkamp, and L. P. Kouwenhoven, Science **281**, 540 (1998).
[5] G. Schedelbeck, W. Wegscheider, M. Bichler, and G. Abstreiter, Science **278**, 1792 (1997).
[6] J. J. Henderson, C. M. Ramsey, E. del Barco, A. Mishra, and C. G., J. Appl. Phys. **101**, 09E102 (2007).
[7] D. Goldhaber-Gordon, H. Shtrikman, D. Mahalu, D. Abusch-Magder, U. Meirav, and M. A. Kastner, Nature **391**, 156 (1998).
[8] L. Kouwenhoven and C. Marcus, Phys. World **11**, 35 (1998).
[9] M. Rontani, F. Rossi, F. Manghi, and E. Molinari, Phys. Rev. B **59**, 10165 (1999).
[10] P. W. Brouwer and I. L. Aleiner, Phys. Rev. Lett. **82**, 390 (1999).
[11] S. Vorojtsov and H. U. Baranger, Phys. Rev. B **72**, 165349 (2005).
[12] D. Goldhaber-Gordon, J. Göres, M. A. Kastner, H. Shtrikman, D. Mahalu, and U. Meirav, Phys. Rev. Lett. **81**, 5225 (1998).
[13] H. Jeong, A. M. Chang, and M. R. Melloch, Science **293**, 2221 (2001).
[14] W. G. van der Wiel, S. D. Franceschi, T. Fujisawa, J. M. Elzerman, S. Tarucha, and L. P. Kouwenhoven, Science **289**, 2105 (2000).
[15] X. Y. Feng Chi and J. Zheng, Nanoscale Research Letters **3**, 343 (2008).
[16] R. Žitko and J. Bonča, Phys. Rev. B **73**, 035332 (2006).
[17] S. Sasaki, H. Tamura, T. Akazaki, and T. Fujisawa, Phys. Rev. Lett. **103**, 266806 (2009).
[18] B. Dong and X. L. Lei, Phys. Rev. B **65**, 241304 (2002).
[19] E. Vernek, N. Sandler, S. E. Ulloa, and E. V. Anda, Physica E: Low-dimensional Systems and Nanostructures **34**, 608 (2006).
[20] E. V. Anda, G. Chiappe, C. A. Büsser, M. A. Davidovich, G. B. Martins, F. Heidrich-Meisner, and E. Dagotto, Phys. Rev. B **78**, 085308 (2008).
[21] R. Schuster, E. Buks, M. Heiblum, D. Mahalu, V. Umansky, and H. Shtrikman, Nature **385**, 417 (1997).
[22] I. Weymann, Phys. Rev. B **75**, 195339 (2007).
[23] P. S. Cornaglia and D. R. Grempel, Phys. Rev. B **71**, 075305 (2005).
[24] L. G. G. V. Dias da Silva, N. P. Sandler, K. Ingersent, and S. E. Ulloa, Phys. Rev. Lett. **97**, 096603 (2006).
[25] J. I. Climente, A. Bertoni, G. Goldoni, M. Rontani, and E. Molinari, Phys. Rev. B **76**, 085305 (2007).

[26] R. Žitko and J. Bonča, Phys. Rev. Lett. **98**, 047203 (2007).
[27] E. Vernek, C. A. Büsser, G. B. Martins, E. V. Anda, N. Sandler, and S. E. Ulloa, Phys. Rev. B **80**, 035119 (2009).
[28] P. Trocha and J. Barnaś, Phys. Rev. B **78**, 075424 (2008).
[29] M. Pustilnik, L. I. Glazman, and W. Hofstetter, Phys. Rev. B **68**, 161303 (2003).
[30] A. K. Mitchell and D. E. Logan, Phys. Rev. B **81**, 075126 (2010).
[31] M. C. Rogge and R. J. Haug, Phys. Rev. B **77**, 193306 (2008).
[32] G. Chiappe, E. V. Anda, L. Costa Ribeiro, and E. Louis, Phys. Rev. B **81**, 041310 (2010).
[33] I. Chan, R. M. Westervelt, K. D. Maranowski, and A. C. Gossard, Appl. Phys. Lett. **80**, 1818 (2002).
[34] A. W. Holleitner, R. H. Blick, , and K. Eberl, Appl. Phys. Lett. **82**, 1887 (2003).
[35] D. T. McClure, L. DiCarlo, Y. Zhang, H.-A. Engel, C. M. Marcus, M. P. Hanson, and A. C. Gossard, Phys. Rev. Lett. **98**, 056801 (2007).
[36] A. Hübel, K. Held, J. Weis, and K. v. Klitzing, Phys. Rev. Lett. **101**, 186804 (2008).
[37] T. Hatano, S. Amaha, T. Kubo, S. Teraoka, Y. Tokura, J. A. Gupta, D. G. Austing, and T. S., arXiv:1008.0071v1 [cond-mat.mes-hall] (2010).
[38] S. Andergassen, P. Simon, S. Florens, and D. Feinberg, Phys. Rev. B **77**, 045309 (2008).
[39] R. H. Chen, A. N. Korotkov, and K. K. Likharev, Appl. Phys. Lett. **68**, 1954 (1996).
[40] T. Ivanov, V. Valtchinov, and L. T. Wille, Phys. Rev. B **50**, 4917 (1994).
[41] V. Kashcheyevs, C. Karrasch, T. Hecht, A. Weichselbaum, V. Meden, and A. Schiller, Phys. Rev. Lett. **102**, 136805 (2009).
[42] V. Moldoveanu, A. Manolescu, and V. Gudmundsson, Phys. Rev. B **82**, 085311 (2010).
[43] M. R. Galpin, D. E. Logan, and H. R. Krishnamurthy, J. Phys.: Condens. Matter **18**, 6545 (2006).
[44] G. Granger, M. A. Kastner, I. Radu, M. P. Hanson, and A. C. Gossard, Phys. Rev. B **72**, 165309 (2005).
[45] C.-H. Chung, G. Zarand, and P. Wölfle, Phys. Rev. B **77**, 035120 (2008).
[46] R. Žitko, Phys. Rev. B **81**, 115316 (2010).
[47] C. A. Büsser, G. B. Martins, K. A. Al-Hassanieh, A. Moreo, and E. Dagotto, Phys. Rev. B **70**, 245303 (2004).
[48] K. G. Wilson, Rev. Mod. Phys. **47**, 773 (1975).
[49] H. R. Krishna-murthy, J. W. Wilkins, and K. G. Wilson, Phys. Rev. B **21**, 1003 (1980).
[50] H. R. Krishna-murthy, J. W. Wilkins, and K. G. Wilson, Phys. Rev. B **21**, 1044 (1980).
[51] R. Bulla, T. A. Costi, and D. Vollhardt, Phys. Rev. B **64**, 045103 (2001).
[52] The occupancy $\langle n_2 \rangle$ of QD2, for $t' = 0$, can be obtained by computing $\langle n_2 \rangle$ for an infinitesimally small t' value and then adiabatically decreasing t' to zero for each set of parameters (e.g., V_g).
[53] A molecular orbital is obtained once the hopping between the two levels ε_1 and ε_2 is strong enough to separate the bonding and antibonding levels (symmetric and antisymmetric combinations, respectively) so that the charge transport occurs through them, and not through the individual levels ε_1 and ε_2. For more details, see Ref. 27.
[54] C. A. Büsser, E. Vernek, P. Orellana, G. A. Lara, E. H. Kim, A. E. Feiguin, E. V. Anda, and G. B. Martins, Phys. Rev. B **83**, 125404 (2011).
[55] The model studied in Ref. 54 consists of two capacitively coupled levels ($|+\rangle$ and $|-\rangle$) that are each coupled to an independent band (by hoppings t_+ and t_-). When t_+ is finite and $t_- = 0$, this model is exactly the same as the one studied here for $t_0 = 0$. As shown in Ref. 54, the $|+\rangle$; $|-\rangle$ model is exactly equivalent to the two-level SU(2) limit of the SU(4) model, which describes the many-body state in carbon nanotube QDs. For more details, see J. S. Lim, M.- S. Choi, M. Y. Choi, R. Lopez, and R. Aguado, Phys. Rev. B 74, 205119 (2006).
[56] P. J. Pemberton-Ross, A. Kay, and S. G. Schirmer, Phys. Rev. A **82**, 042322 (2010).
[57] Note that to determine which state (Kondo or IV) provides a larger energy gain to the system, the authors have used the Density Matrix Renormalization Group to estimate the gain in energy for QD1 in a large window of gate potential (encompassing both regimes). This is thoroughly described in Ref. 54.